Measurement 44 (2011) 65–73

Contents lists available at ScienceDirect

Measurement

journal homepage: www.elsevier.com/locate/measurement

RF CMOS transceiver at 2.4 GHz in wearables for measuring the cardio-respiratory function

João Paulo Carmo *, José Higino Correia

University of Minho, Department of Industrial Electronics, Campus Azurem, 4800-058 Guimaraes, Portugal

ARTICLE INFO

Article history:
Received 31 October 2008
Received in revised form 30 August 2010
Accepted 10 September 2010
Available online 17 September 2010

Keywords:
Heart rate measurement
Respiratory frequency measurement
RF CMOS transceiver
Sensor interface
Wireless sensors networks
Wireless microsystems

ABSTRACT

This paper presents a radio-frequency (RF) transceiver for operation in the 2.4 GHz ISM band. The RF CMOS transceiver can be supplied with only 1.8 V, and it was designed to establish wireless links for distances up to 10 m, for a maximum baud-rate of 250 Kbps with a Bit Error Probability less than 10^{-6}. The transmitter can deliver a output power of 0 dBm with a consumption of only 11.2 mW, while the receiver has sensitivity of −60 dBm and consumes only 6.3 mW. The goal of RF CMOS transceiver is for co-integration with sensors in the same die using microsystems techniques. The target application of such microsystems is in wearables (e.g., in wireless electronic shirts) for measuring biomedical data of patients. The wireless electronic shirt (WES) measures the heart rate and the respiratory frequency, and at the same time it allows patients to maintain their mobility.

1. Introduction

Today, the link between textiles and electronics is more realistic than ever. An emerging new field of research that combines the strengths and capabilities of electronics and textiles into one: electronic textiles or e-textiles is opening new opportunities. E-textiles, also called smart fabrics, have not only wearable capabilities like any other garment, but also have local monitoring and computation, as well as wireless communication capabilities. Sensors and simple computational elements are embedded in e-textiles, as well as built into yarns, with the goal of gathering sensitive information, monitoring vital statistics, and sending them remotely (possibly over a wireless channel) for further processing [1].

In wireless sensors networks, the continuous working time of sensorial nodes are limited by its average power consumption [2]. It is well demonstrated that the RF subsystem is by far the one with the highest power consumption, despite the increased availability of CMOS processes with higher power-consumption efficiencies [3]. In this context, the comparative impact of sensors and electronics (for processing, control and data storage) in the whole power consumption (of wireless nodes) is minimal [4]. The exact implication of the RF subsystem in total power consumption is a topic of increased concern, whose consequence is the increased interest on the definition of new architectures and algorithms [5]. Thus, an RF CMOS transceiver for operation in the 2.4 GHz ISM band with control signals was designed and fabricated to optimize the power consumption. These control signals allows the electronics of control to enable and to disable their blocks. Such a control can be done by switching-off the receiver block when a RF signal is being transmitted, by switching-off the transmitter block when a RF signal is being received, or switch all blocks to put the RF CMOS transceiver in the stand-by mode. The UMC RF 0.18 μm CMOS process was the selected technology to fabricate the RF CMOS transceiver, because RF passive elements can be integrated on the same die: integrated spiral inductors (with a reasonable quality factor, Q, up to 10), high resistor values (a special layer is available) and the possibility to use the low-power supply of 1.8 V. Moreover, this CMOS process gives the possibility to use one polysilicon and six metal layers.

* Corresponding author.
E-mail address: jcarmo@dei.uminho.pt (J.P. Carmo).

0263-2241/$ - see front matter © 2010 Elsevier Ltd. All rights reserved.
doi:10.1016/j.measurement.2010.09.027

2. RF CMOS transceiver design

2.1. Specifications

Fig. 1 shows the block diagram of RF CMOS transceiver, which is composed by a RF receiver, a RF transmitter, a RF switch and a frequency synthesizer (PLL-Phase-Locked Loop). The RF switch is digitally controlled, and it connects the antenna either to the RF receiver or to the RF transmitter [6]. The isolation between non-connected ports on RF switch must be high to avoid undesirable leakages between RF receiver and transmitter. Additionally, the losses between connected ports must be the lowest possible, in order to avoid further amplifications of RF signals. The RF receiver has an envelope detector that performs the down-conversion from the RF band to the base-band. The power budget of the RF CMOS transceiver is settled for the maximum baud-rate of 250 kbps, with a Bit Error Probability (BEP) less than 10^{-6} (BEP $\leqslant 10^{-6}$). This quality of service (QoS) is for a maximum transmitted power, P_t [dB], of $P_T = 0$ dBm (hence, $p_t = 1$ mW) with the Amplitude Shift Keying (ASK) modulation. The environment noise was measured with the help of an antenna with an impedance of 50 Ω (at the central frequency of 2.4 GHz) and a Spectrum Analyzer, model *Agilent E4404-B*. It was observed a maximum noise power of $N = -104$ dB. The QoS and the maximum noise power will help to get the minimum sensitivity of RF receiver. The BEP for ASK systems with envelope detection (also known as non-coherent ASK systems) is given by [7]:

$$\mathrm{BEP} = \frac{1}{2} e^{-\gamma_0/2}, \ \gamma_0 \gg 1 \tag{1}$$

where γ_0 is the signal-to-noise ratio (SNR) at the receiver. The Eq. (1) states a minimum SNR in the receiver site of $\gamma_0 \geqslant 26$ ($\gamma_0 = 14$ dB) to have a BEP $\leqslant 10^{-6}$. The minimum power, P_R [dB] (or p_r [W]), of RF signals in the RF receiver is such that [8] $\gamma_0 = S_{\min} - N \geqslant 14$ dB thus, the sensitivity of RF receiver must be at least equal to $S_{\min}$, e.g., $S_{\min} = 14 + N = -90$ dB Δ−60 dBm.

2.2. Receiver

Fig. 2 shows the schematic of RF receiver. In a typical RF receiver, the LNA is the first gain stage in the receiver path.

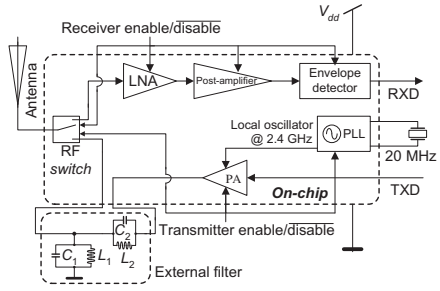

Fig. 1. The block diagram of RF CMOS transceiver at 2.4 GHz.

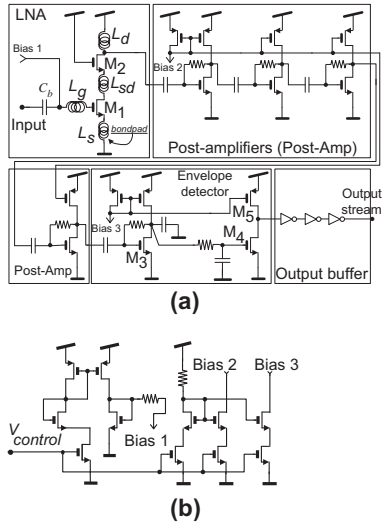

Fig. 2. The schematics of (a) RF receiver; (b) bias and control circuits.

The signal must be amplified as much as possible, with a small signal-to-noise ratio (SNR) decrease (with the lowest noise figure, NF). The LNA is an inductively degenerated common source amplifier [9]. Therefore, the input impedance at 2.4 GHz is equal to 50 Ω for matching with the RF switch. The cascading transistor M_2 increases the gain and simultaneously, it improves the isolation from the output to input and reduces the effect of gate-source capacity, C_{gs}, of M_1. The LNA enters in the sleeping mode, when the current in the polarization stage ceases to flow. The same principle was applied to all subsystems of RF CMOS transceiver. The inductance L_s is made of a bonding connection to the external PCB, whose value was estimated to be 0.9 nH/mm [10]. The wires that connect the die to an external PCB have an inductance that adds to the LNA circuit. The inductance L_{sd} helps to overcome a common effect associated to the bonding pad, which consists on the addition of the inductance in the wires (used to connect the pads in the die circuit to the PCB). The input impedance of LNA is given by [11]

$$Z_{in} = sL_g + 1/(sC_{gs}) + [(g_{m1}/C_{gs}) + sL_s] \tag{2}$$

The input matching is done, by trimming the inductances L_s and L_g. The matching is achieved, when the input impedance is real and equal to the impedance, Z_{ant} [Ω], of the antenna (the 50 Ω is the most common value in the practice). The matching condition is then achieved, when these two conditions are simultaneously verified: $\mathrm{Im}(Z_{in}) = 0$ and $\mathrm{Re}(Z_{in}) = Z_{ant}$ (=50 Ω).

The next step to design a LNA is the calculation of the optimal width of M_1, W_{opt} [μm] [12]. The optimal width is obtained with the following equation:

$$W_{opt} = \frac{1}{6\pi f_c L C'_{ox} Z_{in}} [\mu m] \quad (3)$$

where f_c [Hz], is the central frequency of LNA; L [μm] is the channel length of M_1, C'_{ox} [F m^{-2}] is the gate oxide capacitance and finally, Z_{in} is the input impedance of the LNA, which is desired to be real and equal to 50 Ω. The capacitance is:

$$C_{ox} = \varepsilon_{ox}/T_{ox} \quad (4)$$

where T_{ox} [m] is the SPICE parameter, which defines the oxide thickness [13]. The parameters, $T_{ox} = 4.2 \times 10^{-9}$ m and $\varepsilon_{ox} = 4.1$ $\varepsilon_0 = 4.1 \times 8.85$ aFμm^{-1}, presented in the UMC 0.18 μm RF CMOS process, helps to obtain C_{ox} = 8639.3 aFμm^{-2} = 8.6393 mFm^{-2}. Thus, the optimal width that simultaneously minimizes the consumption and the NF of LNA, is W_{opt} = 284.29 μm. The UMC 0.18 μm RF CMOS process has MOSFET optimized to the operation at high frequencies: the RF transistors. The gate–source capacitance of M_1 is C_{gs} = 830 fF and the transconductance is g_{m1} = 20.27 mS. The values for each of the inductance are L_s = 2.01 nH and L_g = 3.27 nH. The most suitable block capacitance at the input of the LNA is C_b = 10 pF. The observed current at the drain of the transistor M_1 is 2 mA, which is the minimum limit of supply current.

The use of RF components was mandatory during the RF CMOS transceiver design, in order to avoid mismatching problems associated to the passive elements. The values of the previous inductances were obtained for a capacitance, C_{gs}, of a transistor with an arbitrary width $W = W_{opt}$. The UMC foundry allows the fabrication of transistors optimized for RF operation, thus, the component selections felt on these kind of devices due to their low noise and better isolation properties, when compared to those available in the mixed-mode transistors. The width of transistors optimized for operation in RF cannot be any value, in fact, the width is directly related to the number of MOSFET fingers (each finger has a fixed width of 5 μm). Each RF-optimized MOSFET has a maximum number of fingers equal to 21 (thus, the maximum width is limited to 105 μm with 5 μm integer steps). This was the first reason to design the width of M_1 equal to 105 μm, against the optimal value W_{opt}. The second reason, deals with the fact to have a small DC block capacitance C_b = 2 pF that occupies a less chip area when compared with the previous 10 pF, making the capacitor integration in the die of LNA easier.

For W_{opt} = 105 μm, the gate-source capacitances of M_1 and M_2 are C_{gs} = 129.94 fF. After take in account the inductance of bondwires (0.9 nH/mm), the results are an internal source inductance and a transconductance equals to L_{s_int} = 41.2 pH and g_{m1} = 21.28 mS, respectively. These values were calculated for a drain–source voltage of V_{ds} = 1.03 V and with a bias voltage of V_{gs} = 579 mV. After using the Eq. (3) the following external inductances were obtained: L_{s_ext} = 0.264 nH and L_g = 33.5 nH. It must be noted, that $L_{s\_ext} = L_s - L_{s\_int} = R_s \cdot C_{gs}/g_{m1} - L_{s\_int}$.

The gate inductance was further adjusted to a new value, L_g = 21 nH, because it was not possible to achieve a satisfactory gain with the previous value. The inductance, L_{sd}, connected between M_1 and M_2, is 10 nH and it help to increase the gain of LNA, and improving the S_{11} parameter (by lowering the return-loss at the input of LNA). The inductance connected to the drain of M_2, measures L_d = 4.4 nH and makes a tank circuit for 2.4 GHz with a 1 pF capacitance. The inductance L_s is below the minimum allowed by the UMC process, thus, a bondingwire was used to implement this inductor. The inductance L_{sd} is the only one that is fully integrated in the die. All the remaining inductances must take into account the bondwire effect. Then, the actual inductances are slightly smaller (in a quantity equal to 0.9 nH/mm) than those obtained in the theoretical calculations to compensate the bondwire effect. Table 1 shows the components of LNA: the internal inductances and the bondwires [14].

An additional amplifier in the output of LNA provides a RF signal with an amplitude higher than the minimum required by the envelope detector. Basically, the idea of the envelope detector is as follows: an increasing in the input amplifier implies a decrease in the M_3 gate voltage (this keeps the branch current constant), meaning a decrease in the gate voltage of M_4 (after filtering), thus decreasing the transistor M_4 current itself. When this current reaches a point that cancels with the mirrored current in M_5, the output capacitance starts to discharge and the output voltage increases.

2.3. Transmitter

Fig. 3 shows the schematic of complete RF transmitter, which is composed by a power amplifier (PA) and a selection circuit (or power select circuit) that selects the RF power. The power amplifier is of switched type, and it generates the ASK modulated signal. The network L_1–C_1 is a tank circuit tuned to the carrier frequency, and it is used to keep only the 2.4 GHz in its terminal. The network L_2–C_2 reduces the emissions outside the transmitting band with the central frequency of 2.4 GHz.

2.4. Frequency synthesizer

As depicted in Fig. 4, the frequency synthesizer is a Phase-Locked Loop (PLL) that uses the integer division technique. The 2.4 GHz are generated from the reference frequency of 20 MHz. A new type of Phase/Frequency Difference (PFD) circuit makes the PLL faster, when compared to the classical configuration [15]. The Charge Pump (CP) is of current steering type [16]. This circuit avoids the conventional problem in CPs that limits the opening and closing of current sources. In this CP, the current is not switched, but routed from the load to an alternative path and from that path to the load. This reduces the ripple in the input control of the Voltage Control Oscillator (VCO).

Table 1
Components of the LNA.

	Value 1 (nH) On-chip	Q_1 Inductances	Value 2 (nH) Bonding	Q_2 Inductances
L_s			0.305	20
L_g	18.26	8.249	0.9	20
L_{sd}	10.00	7.177		
L_d	3.145	7.177	0.9	20

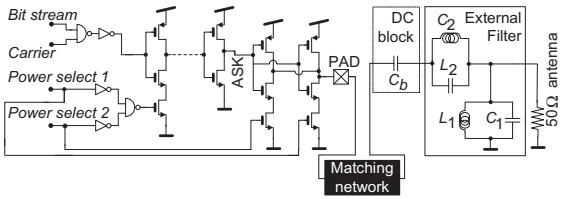

Fig. 3. The schematic of RF transmitter.

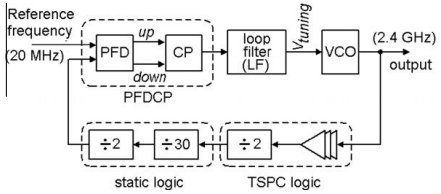

Fig. 4. The PLL structure.

As a consequence, the spurs of the reference are also reduced, and the PLL takes less time to lock.

The VCO is a current starved ring oscillator. This circuit has the advantage to save on-chip area, when compared with tuned LC oscillators, but have more phase noise [17]. For overcoming this limitation, the bandwidth of the PLL is high enough to "clean-up" the output spectrum around 2.4 GHz [18]. A third order passive filter, composed by a second order section (C_1, C_2 and R_2) and a first order section (C_3 and R_3), providing an additional pole it is used. The first order filter reduces spurs caused by the multiples of the reference frequency, which consequence is the increasing of the phase noise at the output. The division by 120 in the feedback path is done with a cascade constituted by one half divider implemented with a True Single Phase Clock (TSPC) logic, one divider by 30, followed by a toggle flip-flop to ensure a duty-cycle of 50% at the PFD input. This circuit requires a rail-to-rail input to work properly [19].

3. Experimental results

Fig. 5 shows a photograph of the first prototype of a low-power/low-voltage RF CMOS transceiver, which has been fabricated in the UMC RF 0.18 μm CMOS process and occupies an area of 1.5 × 1.5 mm^2.

The experimental tests of the RF CMOS transceiver, show a total power consumption of 6.3 mW for the RF receiver (4 mW for the LNA, and 2.3 mW for the envelope detector + post-amplifier), and 11.2 mW for the RF transmitter. The RF transmitter delivers a maximum output power of 1.28 mW (very close to the specified 0 dBm) with a power consumption of 11.2 mW. When enabled, the power at the output of the PA, can be selected from the following values: 0.22 mW, 1.01 mW and

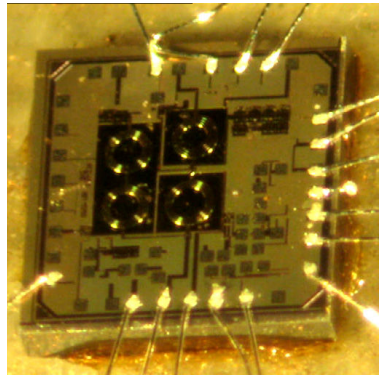

Fig. 5. A die photograph of the RF CMOS transceiver.

1.21 mW. It was observed for the LNA, a S_{21} of 19.2 dB, a NF of 3 dB, a 1 dB compression point (IP1) of −9 dBm, and a third order intercept point (IP3) of −5.4 dBm. Fig. 6 shows the IP1 and the third order intercept point (IP3). The LNA has also a stabilization factor of K = 1.8 (higher than one), that makes this amplifier unconditionally stable.

The CP has a detector constant gain $K\varphi$ = 175 μA/2π rad. The transistor M_2 at the VCO keeps the oscillations on situations where the voltage at the gate of the transistor M_1 falls below the threshold voltage, V_{th}. This makes possible to control the VCO at the full range [0, 1.8 V], providing the frequency range of [2.02, 2.76 GHz], with a tuning constant K_{VCO} = 876.6 MHz/V, calculated in the linear working range (see Fig. 7). The judicious choosing of the loop-filter turns this PLL to lock in only 1.6 μs. This locking time is less than half a bit duration time, at maximum baud-rate of 250 kbps. Finally, the RF switch provides a minimum port-isolation of 41.5 dB and a maximum insertion loss of 1.3 dB, overcoming the reference values [6].

4. Wireless electronic shirt (WES)

4.1. Motivation

World Health Organization (WHO) estimates that 16.7 million people around the globe die of cardiovascular

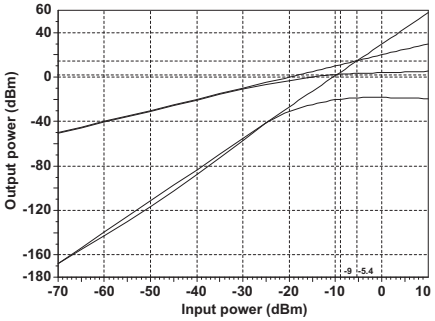

Fig. 6. IP1 and IP3 of LNA.

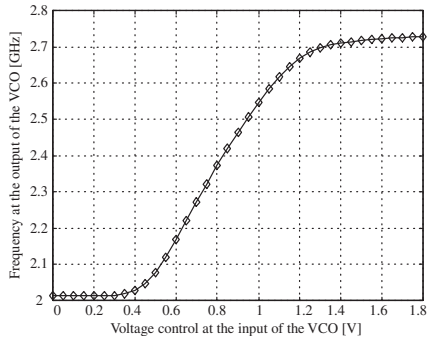

Fig. 7. Measured working characteristic of VCO.

diseases (CVD) each year. Heart attack and stroke deaths are responsible for twice as many deaths in women as all cancers combined. Low- and middle-income countries contributed to 85% of CVD deaths. By 2020 the WHO estimates nearly 25 million CVD deaths worldwide, thus, heart disease has no geographic, gender or socioeconomic boundaries. Moreover, between 1990 and 2020, deaths from non-communicable diseases and injury are expected to rise from 33 million to 58 million annually, with a similar proportional increase in years of life lost. By 2020, cardiovascular diseases, injury and mental illnesses will be responsible for about one half of all deaths and one half of all healthy life years lost, worldwide [20].

Fifty percent of death and disability from CVD can be reduced by a combination of simple effective national efforts and individual actions to reduce major CVD risk factors [20]. On this context, the monitoring of cardio-respiratory function with the wireless electronic shirt (WES) constitutes a breakthrough on this matter. The monitoring is made by simultaneously measuring the heart rate and the respiratory frequency. This makes the WES a powerful tool, helping health professionals with rapid, accurate and sophisticated diagnostics, and allow them to recognize qualitatively and quantitatively the presence of respiratory disorders, both during wake and sleep-time in free-living patients with chronic heart failure, providing clinical and diagnostic significance data.

4.2. WES systems architecture

Like any other every-day garment piece, the wireless electronic shirt (WES) is lightweight, machine washable, comfortable, easy-to-use shirt with embedded sensors. Sensors are plugged into the shirt around patient's chest and abdomen, in order to measure respiratory and cardiac functions. The WES also uses small sizes and compact modules, made with microsystem technology, containing the 2.4 GHz RF CMOS transceiver, the electronics for control and processing, and the interfaces to the sensors. These modules have also an associated antenna and are supplied by a coin-sized battery.

As depicted in Fig. 8a, the communication scenarios found in conventional applications of electronic shirts, use a flexible data bus integrated into the structure, which is used to route the information from the sensors to the controller, and from this one, the information is wirelessly relayed to an external base-station [21]. Examples of such products, includes the shirts found in [22], which are used in remote life-signs monitoring systems for use by fire-fighters, police, industrial clean-up workers or others. Another non-flexible example of wearable [23], is a system used to collect analog signals through conductive fiber sensors and passes them through a conductive fiber grid knitted in a T-Shirt. In this shirt, a textile connector passes the analog signals to a small personal controller held in a pocket on the shirt, then the personal controller digitizes the signal and transmits the signal to a Bluetooth or Zigbee receiver connected to a base-station where the information is further collected and analyzed. The wired concept is a problem when the textiles going to wash, because it requires removal of complex electronics before starting the cleaning process. Another disadvantage is that the topological location of different processing elements is fixed throughout the lifetime of the applications.

The vivometrics's LifeShirt includes sensors that collect signals from freely moving subjects for up to 24 h [24]. The data generated is wirelessly transmitted, by way of a Bluetooth connection, and allows health professionals to monitor and analyze data of up to only sixteen subjects in real-time or to be stored for later analysis. A more interesting application and an easy way to implement wireless buses, is using wireless modules able to communicate between them and between an external base-station (a PDA or a mobile phone). As depicted in Fig. 8b, this solution fits the medical doctor requirements for an easy placement and removal of the wireless modules in the shirt. Moreover, with this solution it is very easy to populate wireless modules in different positions. The sensors can also be removed from the shirt, either when the sensors are no more needed or when the shirt is to be cleaned and washed. This wireless bus introduces the concept of plug-and-play in textiles.

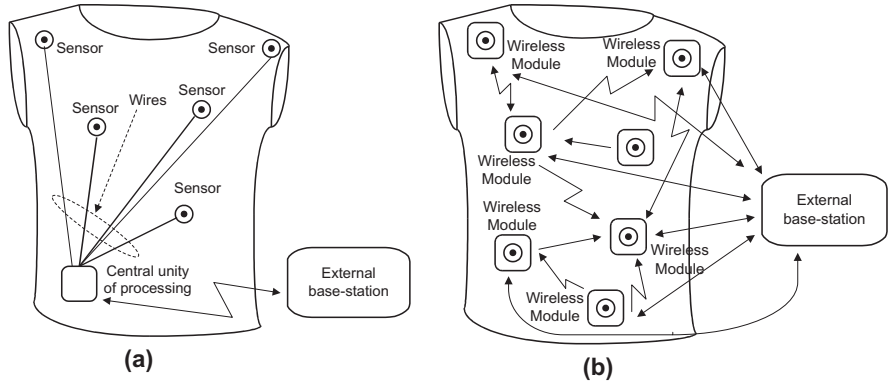

Fig. 8. (a) Conventional application, where wires are used to connect the sensors to a centrally located unity of processing; and (b) the wireless bus mounted in the proposed wireless electronic shirt.

As the data is to be periodically acquired from all of the modules and transmitted to the base-station, the latencies of data transmissions are not allowed. The proposed wireless modules use a communication protocol that overcomes these problems [25]. As illustrated in Fig. 9, two types of frames were defined: the general use and the command frames. The general frames has two purposes, one is to carry information in the payload field between the nodes and the base-station, in a coordination fashion. The second function is sending commands from the base-station to the network nodes. The command frames are used by the base-station to send commands toward the network nodes that were already identified by the base-station. These frames are quickly identified, such as confirmations of good (ACK – Acknowledgements) or bad reception (NACK – Nacknowledgements) of previously received data. In the first frames, the payload length is variable. In the case of sending commands, the field "frame type" is 01 h (00 00 00 01b), the length of the frame is minimum (only nine bytes). The default case is when the frame carries data, e.g., the value in the "type field" is 00 h (00 00 00 00b). In the future, additional types can be defined, by making the "type field" higher or equal to 02 h (00 00 00 10b). These frames, allows to identify the node, for numbering the network and to check with the help of the Cyclic Redundancy Check (CRC) field, the existence of transmission errors.

The WES application is the monitoring of the cardio-respiratory function, where a single-channel for heart rate and an inductive elastic band measures the respiratory function. The ECG signal ranges from a 400 μV to 5 mV peak. In relation to the measurement of the breath rate, a transducer with a variable inductance indirectly measures changes in the thoracic diameter. The device is located in a position around the body at the level of maximum respiratory expansion. At maximum inspiration the belt is

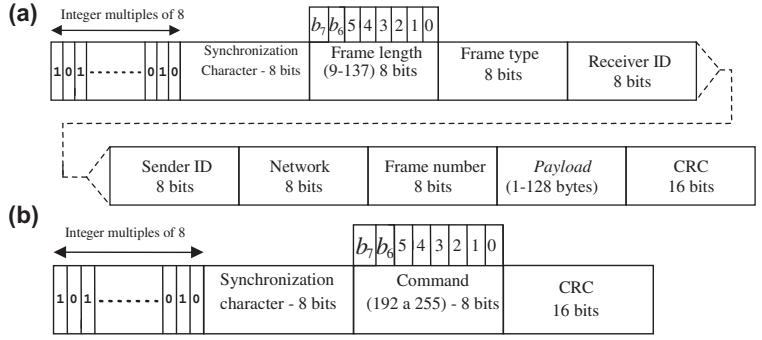

Fig. 9. Existing fields in (a) the general use and in (b) the control frames.

stretched almost to maximum extension, making the inductance minimum. As depicted in Fig. 10, the 20 MHz frequency reference of the PLL can be used in this circuit. The variations in the inductance, changes the attenuation for the 20 MHz signal, in the first *RL* low-pass of first order filter (at Filter 1). Thus, the attenuation increases when the thorax perimeter decreases. This filtered signal is further amplified, before a second low-pass filtering (at Filter 2 in Fig. 10), to eliminate noise and spurs generated in the 20 MHz oscillator. Then, a peak detector gets the amplitude of the 20 MHz processed signal, which is:

$$V_{peak} = \underbrace{\frac{V_{20}.A}{\sqrt{1+w^2C^2R_2^2}}}_{\text{Fixed term}} \times \underbrace{\frac{1}{\sqrt{1+w^2L^2/R_1^2}}}_{\text{Variable term(with } L\text{)}} \quad (5)$$

where $w = 2\pi \times 20 \times 10^6$ [rad s^{-1}] is the angular frequency, V_{20} [V] is the amplitude of the 20 MHz sinusoidal signal and A is the gain of an auxiliary amplifier. The voltage at the output of the peak detector is amplified to cover the entire input range of the analog-to-digital converter (ADC). Also, the former amplifier provides isolation between the two filtering stages, which helps to avoid load-matching problems, when these stages are connected. The signal at the output of the peak detector follows the low-frequency respiration signal and it is converted to the digital domain, using an ADC with an output resolution of 8 bits.

Fig. 11 shows a photo of the patient wearing an WES ready to plug RF modules.

4.3. Impacts of RF transmission on measurements

Two major issues have direct impact in the quality of acquired signals. The first one is related to the wireless communication, where the errors can have several effects in the transmitted data. The less severe effect is when one or more bits in the payload are toggled. The most severe effect is when at least one bit in the address of the destiny node (the "receiver ID" field) is toggled. In this situation, the receiver wrongly discards a frame with data. However, as seen in Fig. 9a, bit changes in other five important fields ("synchronization character", "frame length", "frame type", "network ID" and "frame number") also implies (total or partial) loss of data. For a channel with

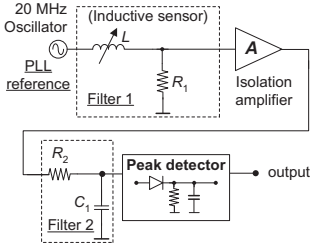

Fig. 10. The block diagram of a signal conditioning used in the measure of the respiratory function.

Fig. 11. A photo of the patient wearing a electronic shirt ready to plug RF modules.

an error probability, BEP, the probability, P_{loss}, to occur a loss of frame due to errors in the former listed fields, is:

$$P_{loss} = \sum_{k=1}^{\text{Total frame length}} C_k^{48} \cdot \text{BEP}^k \approx C_1^{48} \cdot \text{BEP} = 48 \cdot \text{BEP} \quad (6)$$

where C_k^n is the number of k-combinations from a set with n elements. In a data frame, n is the number of sensitive bits, e.g., $n = 6 \times 8$ bits. These are the bits susceptible to generate loss of frames, when errors are present in the channel. Six is the number of important fields in a data frame, where a single error will result in a loss of frame. The maximum specified BEP is 10^{-6} for the RF CMOS transceiver, thus a data frame is lost with an error probability of $P_{loss} = 48 \times 10^{-6}$. It is clear that as high is the lost probability of frames, P_{loss}, the lowest must be the baud-rate, to keep the data transmission more reliable and less risk to errors. For the proposed application, where the sampling frequency do not exceed 100 Hz (heart rate and respiratory frequency are low) the lost of data is not critical.

The second issue is the acquisition time by a node. The acquisition time and the comparison with the processing time is of extreme importance to know the lost of samples. Some assumptions are taken in advance to simplify the analysis: first, it is considered a network with N nodes located d_k [m] (where $k = 1...N_{nodes}$) from the base-station and ready to transmit frames with a length of $N_{oct,k}$ data bytes after few data acquisitions. Also, the summing of the processing times in the transmitter, t_{proc_TX} [s], is constant and equal for all nodes, and the same applies with the processing time of receivers, t_{proc_RX} [s]. If the base-station has enough memory storage capacity, then the baud-rate must be at least:

$$r_b > \frac{13 + \max_k(N_{oct,k}) + N_{ctl} + 2N_{header}}{\frac{1}{f_s} - \frac{2d_k}{c} - 2(t_{proc\_TX} + t_{proc\_RX})} \text{[bps]} \quad (7)$$

where N_{header} is the number of bits in the header, and $c = 3 \times 10^8$ ms^{-1} is the speed of light. The validity of the last equation applies only when $t_{proc\_RX} + t_{proc\_TX} < [1/(2f_s) - d/c]$, which means that the analog sampling frequency, f_s [Hz], cannot exceed $1/[2d/c + 2(t_{proc\_TX} + t_{proc\_RX})]$, or else

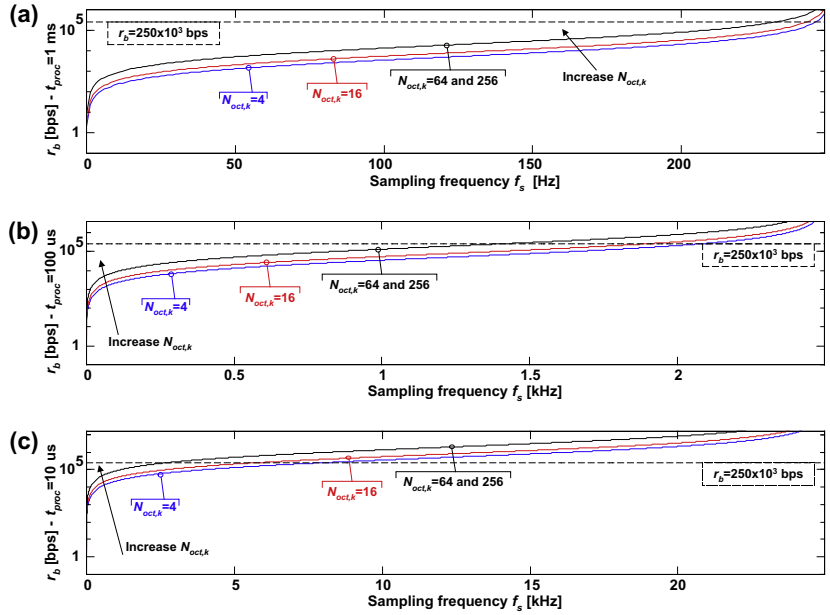

Fig. 12. For three processing times, $t_{proc\_TX} = t_{proc\_RX}$, (a) 1 ms, (b) 0.1 ms and (c) 0.01 ms: the minimum baud-rate, r_b [bps], versus the analog sampling frequency, f_s [Hz], considering data frames whose payload's length, $N_{oct,k}$, are 4, 16, 64 and 256 bytes (these two last situations have similar behaviors, and overlap).

the baud-rate is not high enough to avoid the lost of frames with acquired data.

Three typical scenarios are considered, where the processing times, t_{proc_TX} and t_{proc_RX}, are both equal to 1 ms, 0.1 ms and 0.01 ms. Also, the wireless modules are close to each others (with a distance d_k of 10 m), and the number of bytes in the payload, $N_{oct,k} = \{4, 16, 64, 256\}$ bytes (which corresponds to 1, 4, 16 and 64 samples of 2 analog channels of 2 bytes each). Fig. 12 shows the minimum baud-rate to avoid the lost of frames for several sampling frequencies and simultaneous number of bytes in the payload. From Fig. 12, it is evident that as high is the sampling frequency, the high must be the baud-rate in order to be delivered more data during the same time. Moreover, as the processing time $t_{proc} = t_{proc\_RX} = t_{proc\_TX}$ increases, the high must be the baud-rate, in order to compensate the waste of time during the processing. A dashed line for the maximum baud-rate allowed by the RF CMOS transceiver is also depicted, and serves to illustrate the baud-rate boundary of 250 kbps. Another conclusion is that as high is the number of bytes in the payload, the high must be the baud-rate, in order to not lose again, a frame with data. Another important aspect is the negligible effect of the spacing d_k in the baud-rate, which practically means that t_{proc_RX} and t_{proc_TX} must be smaller than $1/(4f_s)$. These results are promising for the WES application. The measurements of the breath rate and the heart rate are in low-frequency (up to 100 Hz each), thus, it is possible to see that the necessary baud-rate is always below the specified 250 kbps with error probability, BEP, less than 10^{-6} for the RF CMOS transceiver. Moreover, even with high sampling frequencies (as is the case of 2500 Hz for high-resolution ECGs), it is still possible to send long packets of data. However, the electronics must be fast enough to have low-processing times.

5. Conclusions

This paper presented a RF CMOS transceiver, which has been optimized and fabricated in the UMC RF 0.18 μm CMOS process. This transceiver consumes 6.3 mW in the receive mode and delivers 0 dBm with a power consumption of 11.2 mW in the transmitting mode. These characteristics fulfill the requirements for short-range communications for using the 2.4 GHz ISM band.

The main goal of the fabricated RF CMOS transceiver is in wearables, e.g. wireless electronic shirt (WES) for the monitoring of biomedical data in patients while at the same time preserves theirs mobility and lifestyle. Moreover, it will be expected that these kind of applications, will facilitate the diagnostic and will help to reduce the healthcare costs.

Measurements applied to the WES application show minor effects of the errors and the analog sampling process in the lost of data frames.

References

[1] D. Marculescu et al., Electronic textiles: a platform for pervasive computing, Proc. IEEE 91 (12) (2003) 1995–2018.

[2] E. Mackensen, et al., Enhancing the lifetime of autonomous microsystems in wireless sensor actuator networks (WSANs), in: Proc. of the XIX Eurosensors, Barcelona, Spain, 11–14 September 2005.

[3] C. Enz, et al., Ultra low-power radio design for wireless sensor networks, in: Proc. of the IEEE International Workshop on Radio-Frequency Integration Technology: Integrated Circuits for Wideband Communication and Wireless Sensor Networks, Singapore, November 2005.

[4] J. Gutierrez, et al., IEEE 802.15.4: developing standards for low-power low-cost wireless personal area networks, IEEE Network, 2–9 September 2001.

[5] S. Bicelli, et al., Implementation of an energy efficient wireless smart sensor, in: Proc. of the XIX Eurosensors, TC3 1–2, Barcelona, Spain, 11–14 September 2005.

[6] M. Ugajin et al., A 1-V CMOS SOI bluetooth RF transceiver using LC-tuned and transistor–current–source folded circuits, IEEE Journal of Solid State Circuits 39 (4) (1997) 745–759.

[7] B. Carlson et al., Communication Systems – An Introduction to Signals and Noise in Electrical Communications, fourth ed., McGraw-Hill, 2001.

[8] J. Parsons, The Mobile Radio Propagation Channel, second ed., John Wiley and Sons, 2000.

[9] T. Yao et al., Algorithmic design of CMOS LNAs and PAs for 60 GHz radio, IEEE Journal of Solid-State Circuits 42 (5) (2007) 1044–1057.

[10] F. Alimenti et al., Modeling and characterization of the bonding-wire interconnection, IEEE Transactions on Microwave and Techniques 49 (1) (2001) 142–150.

[11] M. Martins, et al., Multi-band combined LNA and mixer, in Proc. of the IEEE International Symposium on Circuits and Systems, May 2008, pp. 920–923.

[12] D. Shaeffer, T. Lee, A 1.5-V, 1.5-GHz CMOS low-noise amplifier, IEEE Journal of Solid-State Circuits 39 (4) (2004) 569–576.

[13] UMC 0.18 μm 1P6M Logic Process Interconnect Capacitance Model, UMC Spec. No. G-04-LOGIC18-1P6M-INTERCAP, Ver 1.7, Phase 1, August 2001.

[14] UMC 0. μm 1P6M Salicide Mixed-Mode/RF CMOS Model, UMC Spec. No. 04UI-02034, Ver 2.2, March 2002.

[15] B. Kim, L. Kim, A 250-MHz–2-GHz wide-range delay-locked loop, IEEE Journal of Solid-State Circuits 40 (6) (2005) 1310–1321.

[16] H. Chin-Ming, K.O. Keneth, A fully integrated 1.5 V 5.5-GHz CMOS phase-locked loop, IEEE Journal of Solid-State Circuits 37 (4) (2002) 521–525.

[17] A. Abidi, Phase noise and jitter in CMOS ring oscillators, IEEE Journal of Solid-Sate Circuits 41 (8) (2006) 1803–1816.

[18] F. Gardner, Charge pump PLL, Transactions on Communications 28 (1980) 1849–1859.

[19] S. Pellerano et al., A 13.5 mW 5-GHz frequency synthesizer with dynamic logic frequency divider, IEEE Journal of Solid-State Circuits 39 (2) (2004) 378–383.

[20] International Cardiovascular Disease Statistics. American Heart Association e-book, pp. 1–14. <http://www.americanheart.org/>.

[21] J. Coosemans, et al., Integrating wireless ECG monitoring in textiles, in: Proc. of the Transducers 05, Seoul, South Korea, 5–9 June 2005, pp. 228–232.

[22] S. Edwards, Health and Safety Guidelines for First Firefighter Training, University of Maryland, Centre for Firefighter Safety Research and Development. Maryland Fire and Rescue Institute, College Park, Maryland, 2006.

[23] E. Batista, Look smart by wearing this shirt, Wired Magazine (2001).

[24] Vivometrics Incorporates Bluetooth Wireless Technology into Lifeshirt Preclinical System. Vivometrics Inc., 20th August 2007, pp. 1–2.

[25] J.P. Carmo, et al., A Low-Cost Wireless Sensor Networks for Industrial Applications, in: Proc. of the Wireless Telecommunications Symposium – WTS 2009, Praha, Czech Republic, April 2009, pp. 1–4.